Capacitive Body-Coupled Communication in the 400–500 MHz Frequency Band

Robin Benarrouch[1,2,3(✉)], Arno Thielens[3,4], Andreia Cathelin[1], Antoine Frappé[2], Andreas Kaiser[2], and Jan Rabaey[3]

[1] STMicroelectronics, Technology and Design Platforms, 38920 Crolles, France
robin.benarrouch@st.com
[2] Univ. Lille, CNRS, Centrale Lille, ISEN, Univ. Valenciennes, UMR 8520 - IEMN, 59000 Lille, France
[3] University of California Berkeley, Berkeley, CA 94704, USA
[4] Ghent University, imec, Department of Information Technology, 9052 Ghent, Belgium

Abstract. One approach to enable wireless communication between body-worn nodes is to use capacitive body-coupled communication (C-BCC). This technique, which uses capacitive electrodes as transducing elements, has previously been demonstrated at relatively low frequencies (<200 MHz) and hence also low bandwidths. This work presents a theoretical analysis of wireless C-BCC, between body worn electrodes at higher frequencies (420–510 MHz), offering the potential for higher data rates. The theory is confirmed both by numerical simulations (performed on a human body phantom), and actual wireless communication between two prototypes on the arm of a real human.

Keywords: Body area network · Capacitive Body Coupled Communication · Radio frequency · Propagation

1 Introduction

Body Area Networks (BAN) are an attractive field of research with a wide variety of applications, including medical- and wellness-oriented systems. A standard for wireless radio-frequency (RF) communication in BANs exists [11]. In this standard, communication within BANs are split in four categories: (1) on-body to in-body to enable the communication with an implanted device; (2) implant to implant communication, (3) on-body to off-body to upload data to a base station for instance, and (4) on-body to on-body communication allowing data exchange between two points over the human body [11].

An interesting concept within BANs, the Human Intranet, introduced in [19], describes the minimum requirements to implement a network dedicated to the human body. The dynamic variations of shape and geometry of such a network raise the need for coverage robustness and reliability. As the network

L. Mucchi et al. (Eds.): BODYNETS 2019, LNICST 297, pp. 218–235, 2019.
https://doi.org/10.1007/978-3-030-34833-5_18

will be connecting a diverse assortment of sensors and actuators (movement, temperature sensors, smart prosthetics, insulin pumps...) with different needs in terms of data rate and latency, a target of multiple tens of Mbps is required in terms of aggregated data rate. Ultimately, the communications must be secured due to the sensitive nature of the transmitted information.

Multiple technical solutions, like standardized RF (Bluetooth...) [6,11], ultrasonic [4], optical [8] or Body Coupled Communication (BCC) [3] could be considered to implement such a system. This manuscript will focus on the latter and more specifically on Capacitive Body Coupled Communication (C-BCC), analyzing and exploring its propagation mechanism. One of the main advantages of C-BCC is the convenient form factor of the on-body capacitive electrodes used for this technology in comparison to on-body antennas which operate at the same frequency. Consequently, this work can be situated in the fourth category described in the IEEE BAN standard [11]. Several papers have already studied and described C-BCC at lower frequencies (below 200 MHz) [1,2,5,13,14,17], with relatively large electrode form factor [2,5,13,14]. Only [13] performed electromagnetic simulations to analyze the impact of the reference electrode on the channel loss in a single on-body configuration. However, up to date, most systems are either impractical for real on-body usage or operate at a carrier frequency that is not high enough to provide the necessary bandwidth and data rates required for the Human Intranet. Therefore, this manuscript focuses on exploring C-BCC using relatively compact electrodes at carrier frequencies higher than the state of the art. Pushing RF communication to higher frequencies does come at a cost: propagation distances will become larger relative to the smaller wavelengths, which in general leads to higher propagation losses at a fixed (on-body) distance [18]. Additionally, the tissues that make up the human body show RF losses that increase over frequency [10]. These considerations led us to target a frequency range of 420–510 MHz offering a good compromise between bandwidth availability and on-body propagation loss [11].

The novelties and main contributions of this manuscript are the following: first, a demonstration of C-BCC at a higher frequency range of investigation than what has previously been demonstrated in literature: 420–510 MHz, second this study on C-BCC considers the theory, numerical simulations, prototyping, measurements and correlates the results.

2 Theory and State of the Art

Capacitive coupling can occur between at least two pieces of conductive material which are not connected together, one used as a reference (called the "reference electrode") and the other(s) connected to the signal feed (referred as the "signal electrode(s)"), see Fig. 1. When another electrode pair is in proximity of such a pair of electrodes there will be coupling between both capacitive electrode pairs. This coupling occurs via several paths. In C-BCC the most common configuration is a stacked architecture where the signal electrode is in contact or in close vicinity to the surface of the body while the reference electrode is stacked on top, both electrically insulated by a dielectric material (see Fig. 1).

A very common way of representing C-BCC in this point of view, is to assume a capacitive return path between both reference electrodes (one on each end, the transmitter (Tx) and the receiver (Rx)) which are floating and an external reference plane, usually the earth ground, as pictured in Fig. 1. In [7] the authors investigated and highlighted the conditions in terms of frequency range and distances under which no power is radiated out of the human body in this configuration. In other words, the conditions where the assumption illustrated in Fig. 1 is applicable. The authors of [7] concluded that the frequency of operation must be below 21 MHz (which is not compatible with the envisioned project highlighted in Sect. 1) in order to keep the communication confined within the human body.

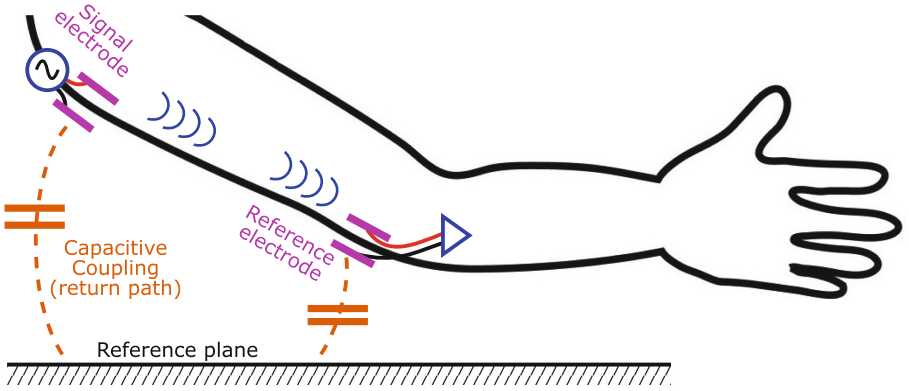

Fig. 1. Common representation of Capacitive Body Coupled Communication mechanism.

Besides this capacitive coupling, there is also electromagnetic wave propagation between both pairs of electrodes. In this aspect, the electrodes can be described as electrically small dipoles at wavelengths that are relatively large in comparison to the electrode dimensions [3]. In free space, there exists a theoretical formulation for the magnitude of the electric field E_z in the plane (XY) (see Fig. 2) at a distance r from such a source (dipole parallel to the Z axis in a Cartesian coordinate system at z = 0) [3]:

$$|E_Z| = \left| \frac{I \cdot dz \cdot k^3}{4\pi\omega\epsilon_0} i \left[\frac{1}{r} + i \cdot \frac{1}{r^2} - \frac{1}{k} \cdot \frac{1}{r^3} \right] \cdot e^{-ikr} \right| \tag{1}$$

With I the current fed to the dipole, dz the length of the dipole, k the magnitude of the wave vector, ω the angular frequency and ϵ_0 the permittivity of free space. When r is relatively small, the $1/r^3$ term is dominant. On the contrary, the term $1/r$ is dominant further away from the source.

The electromagnetic fields surrounding such a small dipole on an infinite conductive surface located at z values below the Z-coordinate of the bottom

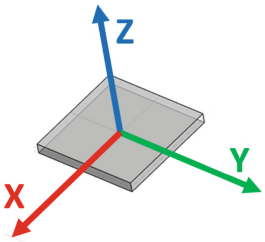

Fig. 2. Parallel plate capacitor in free space centered in a Cartesian coordinate system.

electrode, see Fig. 2, can be expressed theoretically [15,16]. The amplitude of the electric field strength (Ez) at the interface between air and the conducting surface in the direction parallel to the dipole (the dominant polarization [15], when the receiver is also located at the air-conductor interface, the Z direction in Fig. 2) at a distance r from the transmitting dipole can be expressed using [3]:

$$|E_Z| = 2|k \cdot S \cdot \frac{1}{r} + i \cdot \frac{1}{r^2} - \frac{1}{k} \cdot \frac{1}{r^3}| \tag{2}$$

where S is a term that depends on the frequency and the dielectric properties of the conducting surface. The first term in 1/r corresponds to surface wave propagation, while those in $1/r^2$ and $1/r^3$ highlight the induction field and quasi-static coupling respectively. By plotting the weight of those different propagation mechanisms at the frequency range of interest (i.e. 400–500 MHz), it is clear that the surface wave becomes dominant when the distance considered is greater than 13–15 cm. The results are shown in Fig. 3 for S computed for muscle tissue with parameters obtained from the Gabriel database [10].

The theories and investigation on C-BCC described above suggest that we will operate using a communication mechanism dominated by surface wave propagation. This can be advantageous as the communication is less sensitive to changes in the return path. In addition, [7] shows the limits of the representation shown in Fig. 1, and highlights that our electrodes cannot be modeled as an electric circuit only but requires a full-wave electromagnetic simulation to describe the transmission.

3 Materials and Methods

3.1 Numerical Simulations

In order to verify whether the proposed theory [3,15,16] corresponds to transmission between two body-worn electrodes in our studied frequency band (420–510 MHz), we executed two types of numerical simulations: (1) simulations with electrodes in free-space, and (2) simulations with electrodes on a so-called

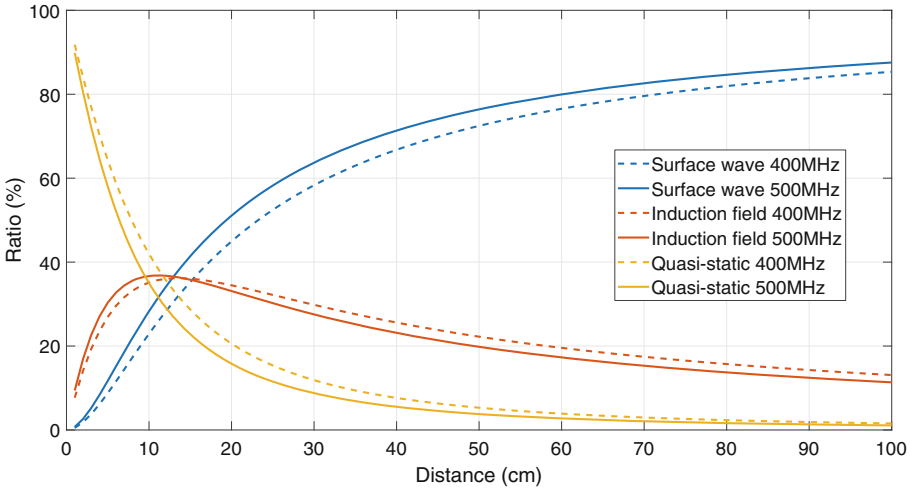

Fig. 3. Contribution of each mechanism as a proportion of the total electric field for 400 MHz (dotted lines) and 500 MHz (solid lines).

phantom. A phantom is a proxy for the human body; in this case, we chose to work with a cuboid that mimics the limbs of the human body.

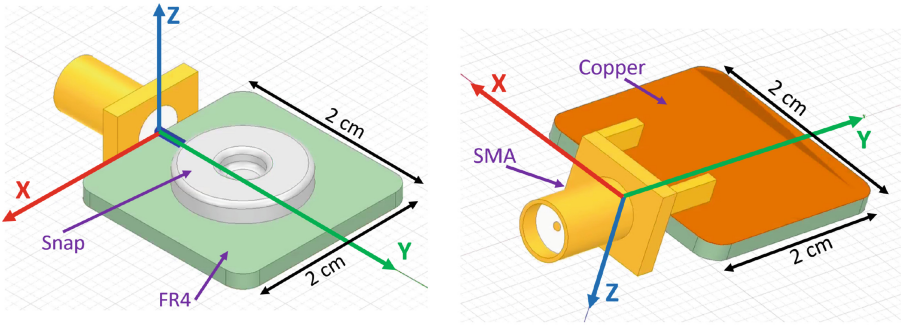

(a) (b)

Fig. 4. 3D electrode model. (a) top view, (b) bottom view.

Figure 4 shows the model of the studied electrodes. The dielectric properties assigned to the different layers were taken from software Ansoft HFSS. The model consisted out of a $2 \times 2\,\text{cm}^2$ FR4 (Relative permittivity = 4.4, Relative Permeability = 1 Bulk conductivity = 0 S/m) board substrate, 1.6 mm thick, covered by a 35 µm copper (Relative permittivity = 1, Relative Permeability = 0.99,

Bulk conductivity = $5.8 \cdot 10^7$ S/m) layer on one side. On the other face, a stainless steel (Relative permittivity = 1, Relative Permeability = 1, Bulk conductivity = $1.1 \cdot 10^6$ S/m) snap connector with a diameter of 12 mm and 1 mm in height was glued. The snap was connected to the central conductor of a side-mounted SMA connector modeled in brass (Relative permittivity = 1, Relative Permeability = 1, Bulk conductivity = $1.5 \cdot 10^7$ S/m), while the connectors ground pads were connected to the copper layer on top of the FR4 board. The SMA and the snap were connected together with a copper wire of 0.8 mm in diameter. The female snap connector was connected to its male counterpart (also modeled as stainless steel). This male snap connector was in its turn connected to a wet electrode (modeled from a standard pre-gelled disposable medical electrode from Covidien: Kendall Arbo H124SH [21]) which was modeled as a conductive dielectric with properties and water (Relative permittivity = 81, Relative Permeability = 0.99, Bulk conductivity = 0.01 S/m).

The phantom is a cuboid shape, with a $50 \times 50\,\text{mm}^2$ square section and a length of 4 m (see Fig. 5). This latter value was selected, so that no simulation artifacts from the edges are observed. The section dimensions were chosen to represent a human arm. The phantom was assigned frequency-dependent dielectric properties corresponding to muscle in the Gabriel database [10].

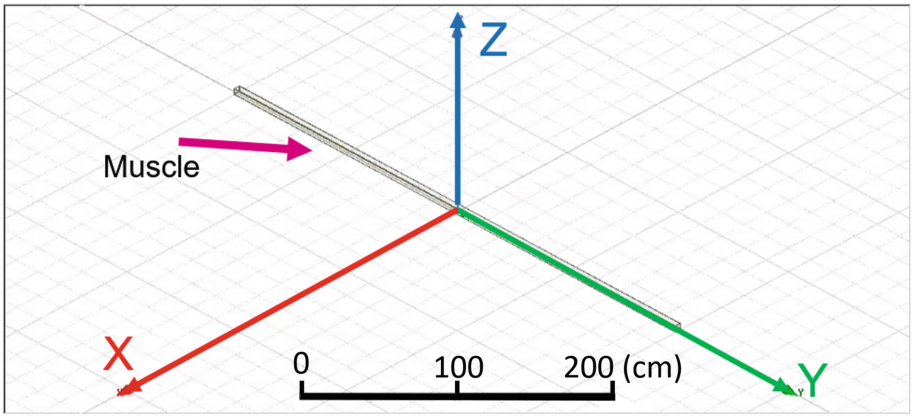

Fig. 5. 3D representation of the cuboid shaped phantom.

In our simulations, the elements of interest (electrodes and arm) are surrounded by a box of air of the following size: $3 \times 3 \times 6\,\text{m}^3$. These electrodes were excited by a lumped port with impedance 50 Ω and voltage 1 V, placed in between the coaxial conductor and the mantle of the SMA connector. The FEM method implemented in Ansoft HFSS was used to calculate the electromagnetic fields surrounding the electrodes when they were fed a voltage at a frequency of 300–600 MHz.

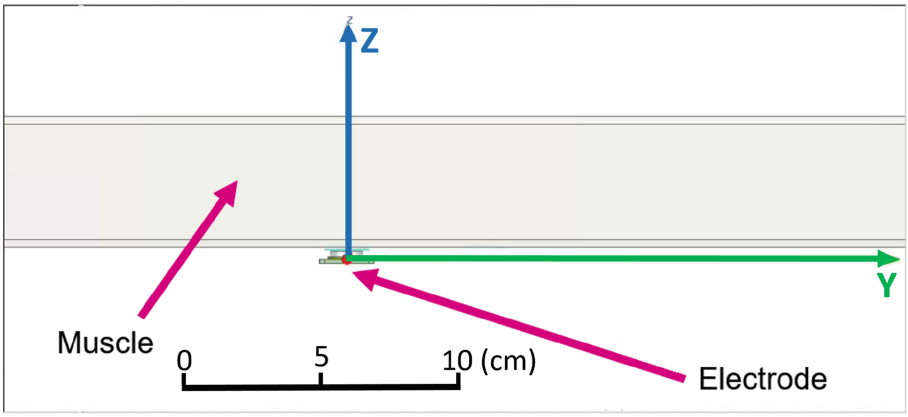

Fig. 6. Electrode positioned on muscle (YZ) plane.

The frequencies of interest were set every 50 MHz from 300 MHz to 600 MHz. In parallel, an interpolating frequency sweep over the same range with 10 MHz steps was enabled. We retained values in the 420–510 MHz frequency band.

3.2 Measurement Set-Up

In order to measure the attenuation under realistic conditions, a fully battery-powered prototype was implemented. Battery-powered operation is key for a standalone wireless on-body application. Moreover, this solution allows for a separation between the two reference planes, which cannot be achieved by connecting those with two cables to the same measurement instrument [1], even with the introduction of baluns in the measurement circuit. In order to achieve flexibility, adaptability and repeatability the signal was generated and controlled with a sub-GHz radio available with the following evaluation kit: STEVAL-FKI433V2 [22] from STMicroelectronics. The signal type was a continuous wave (CW) at a frequency swept from 420 MHz to 510 MHz by steps of 10 MHz.

The electrodes (connector and skin pre-gelled) are shown in Fig. 7.

Lastly, the on-body measurements were performed along the arm of a male subject, standing still, and arms along the body. The transmitter (Tx) was positioned on the left wrist. The receiver (Rx) was placed on the same arm, at a distance d from Tx. The covered range was the following: 5 cm to 55 cm by steps of 5 cm. For every step, the received power at the Rx was computed by collecting 220 samples for frequencies from 420–510 MHz in steps of 10 MHz. These measurements were split for each harmonic frequency and fed into a log-linear least-square fit according to the following channel loss (L) model [3]:

$$L = \begin{cases} L_0 & d = d_0 \\ L_0 + \alpha_0(d - d_0) & d_0 < d < d_1 \\ L_1 + \alpha_1(d - d_1) & d_1 < d \end{cases} \tag{3}$$

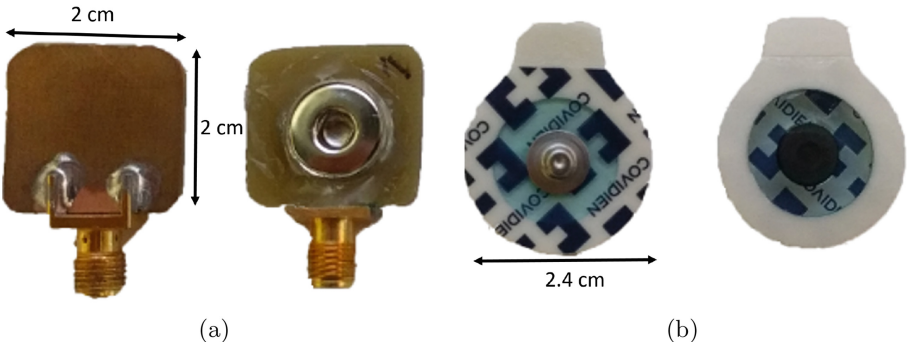

Fig. 7. C-BCC electrode. (a) connector (2×2 cm), (b) skin pre-gelled.

with d the inter-electrode distance, L_0 the baseline channel loss at the shortest measured inter-electrode distance (d_0, 5 cm in this case), d_1 is the boundary distance where the transition between the quasi-static (QS) and surface wave regimes occur. Following the analysis shown in Fig. 3, a boundary distance $d_1 = 15$ cm was determined for the studied frequencies on muscle. Hence, this value was chosen in the fit to determine the channel losses per unit distance α_0 and α_1 in both regimes.

The setup, hardware and measurement conditions were strictly identical to the one described in [20].

4 Results and Discussion

4.1 Free Space Simulation Results

In order to understand the electrode behavior, a single electrode was simulated in the air. The simulation parameters were those described in Sect. 3.1. All plots and figure are in the plane (YZ) (see Fig. 5) since the electrodes are symmetric (except for the SMA) and such representation eases the comparison with the simulation on the phantom.

Figure 8(a) shows the electric field (E-field) radiated by the electrode in air at 450 MHz. The magnitude of the E-field is maximum in the center and fades as the distance increases. Figure 8(b) shows the E-field strength along the positive Y-axis together with two fits: a near field approximation using $1/r^3$ and a far field approximation using $1/r$.

According to theory, the electrode should behave as a small electric dipole in free space with electric field strength according to Eq. (1) with the $1/r^3$ term dominating the near field and the $1/r$ term dominating the far-field behavior. The simulation results highlighted in Fig. 8(b) show a good agreement with the theory presented in Eq. 1 since there is a good correspondence between the fits and the simulation results Fig. 8(a) shows that the magnitude of the E-field is the greatest in the direction parallel to the conductive material (XY plane).

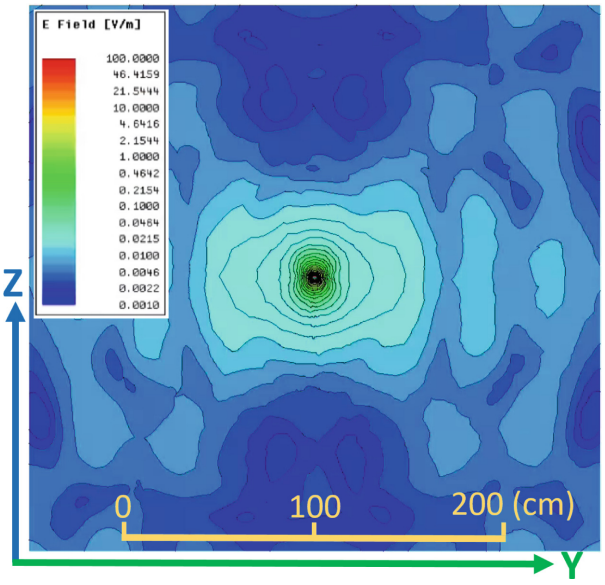

(a)

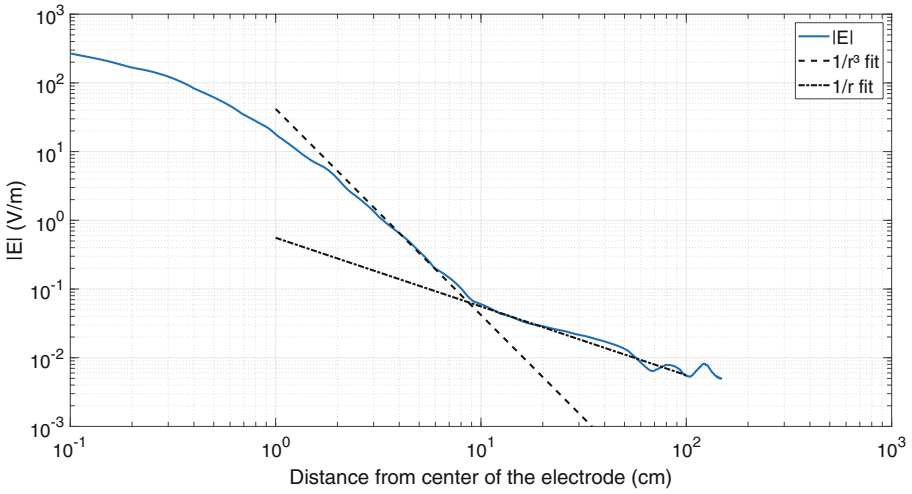

(b)

Fig. 8. E-field radiated by one electrode in air at 450 MHz, (a) in the (YZ) plane, (b) along the positive Y-axis.

Hence, this is the direction of optimal communication. This is in line with the envisioned communication strategy outlined in Fig. 1 and thus shows that these electrodes are good candidates for C-BCC.

4.2 "On-phantom" Simulation Results

The "on-body" simulations were based on the same configuration as the free-space simulation for comparison purposes. A cuboid modeled as muscle was added as described in Sect. 3.1. The electrode was positioned in contact below the muscle, as described Fig. 6.

Figure 9 represents the E-field in the (YZ) plane while a single electrode was positioned on-body at 450 MHz. From this figure, we can observe that in the Y direction the E-field travels further distance than in free-space. For example at 50 cm from the center of the electrode the E-field strength at 450 MHz is 0.26 V/m on the phantom and 0.01 V/m in free space, for the same input power.

As the simulation was conducted in the exact same condition than in free-space, it is clear that the E-field propagates along the phantom model. The electric fields also penetrate the muscle phantom. Figure 9 demonstrates that the fields inside the phantom are out of phase with the ones outside the phantom. The minima of the internal E-fields occur at those propagation distances where the external fields show a local maxima and vice versa.

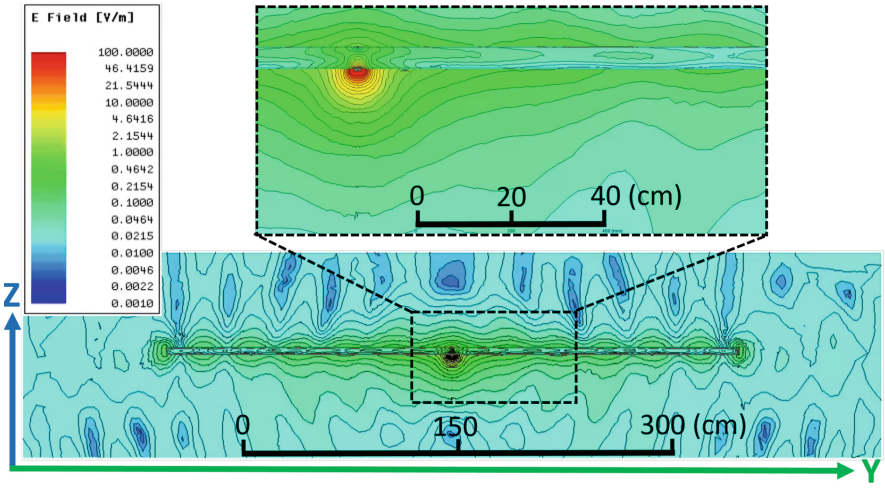

Fig. 9. E-field radiated by a single electrode on muscle at 450 MHz in the (YZ) plane.

For the standard phantom size ($50 \times 50 \times 4000\,\text{mm}^3$), multiple frequencies of excitation from 420 MHz to 510 MHz by steps of 30 MHz were simulated. We performed a comparison between theory (Eq. 2) and simulation of an electrode positioned on a phantom modeled as a cuboid shape with muscle dielectric properties. These results are highlighted Fig. 10 which shows the electric field along the Y-axis for the specified frequency set. Additionally, two fits are shown for

the results at 450 MHz, $1/r$ for the surface wave and $1/r^3$ for the quasi-static field.

The far-field electric field at 450 MHz showed a $1/r$ dependency (Fig. 10) and matches the theory. However the simulation in the near field is only accurate in a very limited range (3 to 5 cm). This could be explained by the electrode's edge positioned at 1 cm from the center, whereas the theory assumes the dipole does not have any width. The E-field strength at a fixed distance for the frequencies of interest (420 MHz to 510 MHz) showed very little fluctuation, less than a factor of 1.5.

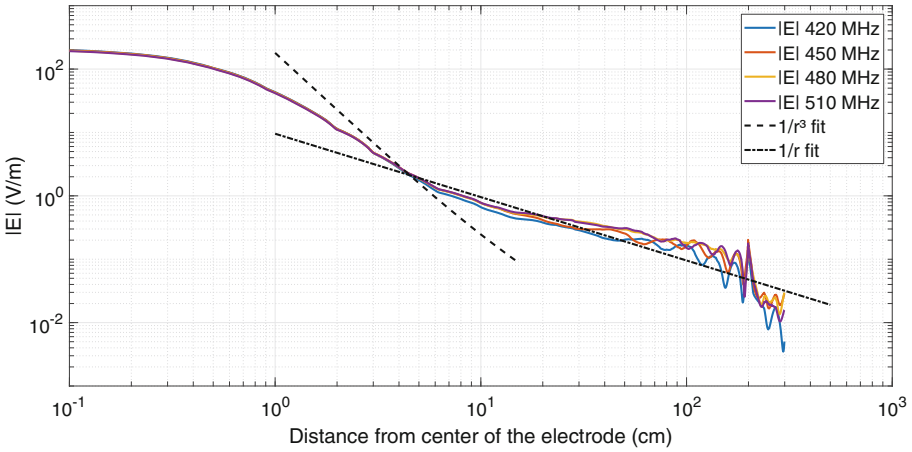

Fig. 10. E-field along the Y-axis radiated by a single electrode on muscle for multiple frequencies on a $50 \times 50\,\text{mm}^2$ phantom cross section.

Figure 11 shows the E-field strength at 5 distances along the Y-axis over the full studied frequency band.

The E-field strength at a fix distance for the frequencies of interest (420 MHz to 510 MHz) showed very little fluctuation, less than a factor of 1.5. This is a desirable property of the communication channel, since this indicates that for a fixed human body limb size a 90 MHz band width with very small fluctuations in channel loss might be available. In order to validate whether this is also the case in reality, these results will be compared with on-body measurements results within the next sub-Section.

In our simulations, the human is represented as a cuboid modeled with the dielectric properties of muscle. Its base-dimensions are $50 \times 50 \times 4000\,\text{mm}^3$ as described Sect. 3.1. However, the arbitrary section size may vary from body to body. In order to better understand the impact of such a variation, the section side-length (as it is a square) was swept from $30 \times 30\,\text{mm}^2$ to $80 \times 80\,\text{mm}^2$ by steps of 10 mm in square edge size. The results are presented Fig. 12.

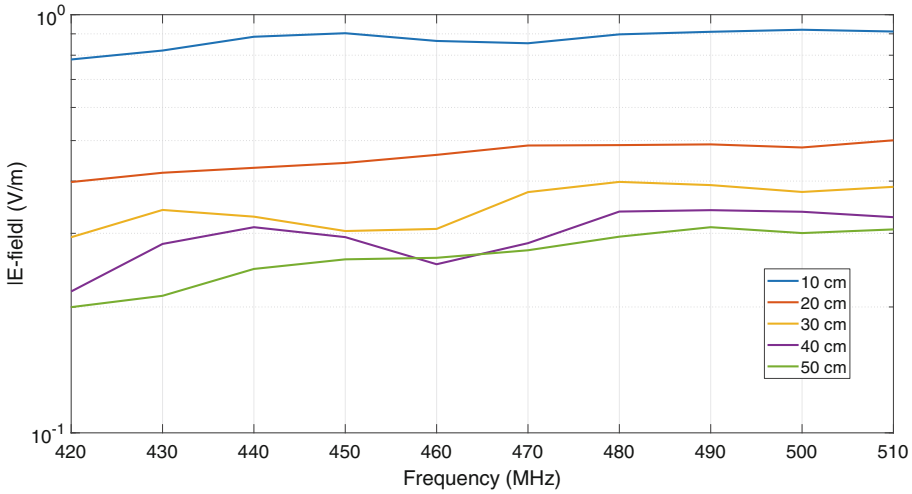

Fig. 11. E-field radiated along the Y-axis by a single electrode on muscle over frequency for multiple distances.

The variations observed in electric field strength are larger when the phantom's section changes at a fixed frequency in comparison to changing the frequency for a fixed section. For example at 50 cm from the electrode, a change in frequency from 420 to 510 MHz, results in a maximal difference of a factor 1.5. On the other hand, at a fixed frequency of 450 MHz we see changes up to a factor of 5 if the phantom's section is changed from $30 \times 30\,\text{mm}^2$ to $80 \times 80\,\text{mm}^2$. These results suggest that the factor S in Eq. 2 does not only depend on the dielectric properties as suggested in [3] but also on the geometry of the phantom.

The polarization of the E-field at the interface air/muscle is plotted in Fig. 13. More than 98% of the total magnitude of the E-field is contained along the Z component of E for propagation distances <200 cm which will be approximately the maximal propagation distance on most human bodies. This shows a strong polarization of the E-field and consequently of the electrode according to the Z direction. It is worth noting that the Z direction in our design is perpendicular to both conductive plates forming the electrode This is again in agreement with the theory presented in Sect. 2.

4.3 On-Body Measurement Results

Figure 14 shows the measured channel losses at 450 MHz as a function of distance along the arm of the subject. The baseline channel loss at 5 cm L_0 is $-47\,\text{dB}$, while the loss at the transition point $L_1 = -55\,\text{dB}$. The fit resulted in two distinctly different slopes defined by the channel losses per distance $\alpha_0 = -0.94\,\text{dB/cm}$ and $\alpha_1 = -0.37\,\text{dB/cm}$. The standard deviation (σ, see

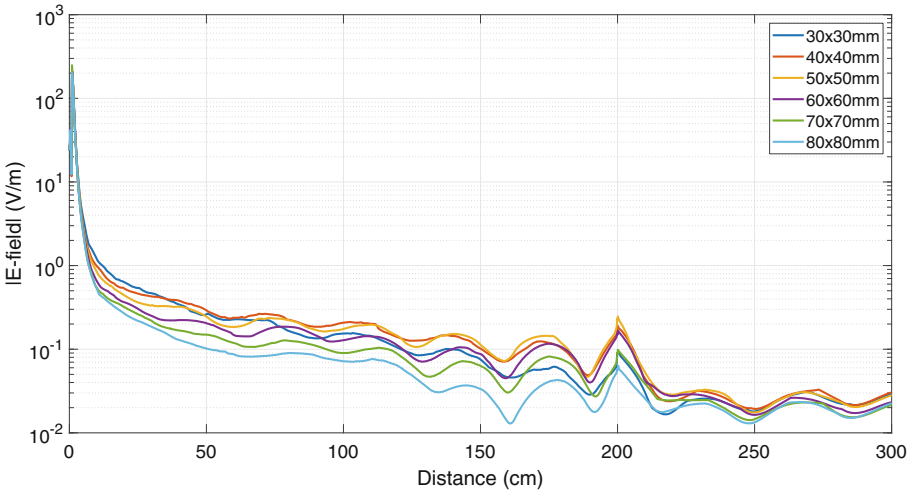

Fig. 12. E-field radiated by a single electrode along the Y-axis on muscle for multiple phantom cross sections at 450 MHz.

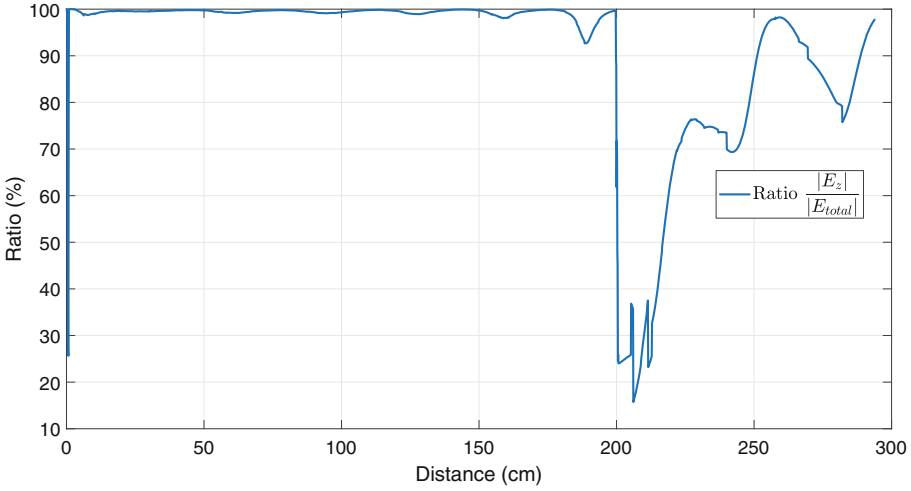

Fig. 13. Ratio of the total electric field along Z direction at 450 MHz with the electrode positioned on muscle.

Eq. 3) on the channel loss model is 6.5 dB. The results of this fit are in line with the model proposed in Eq. 2 with a dominant QS wave near the electrodes that decays stronger over distance than the surface wave which is dominant further away from the electrodes.

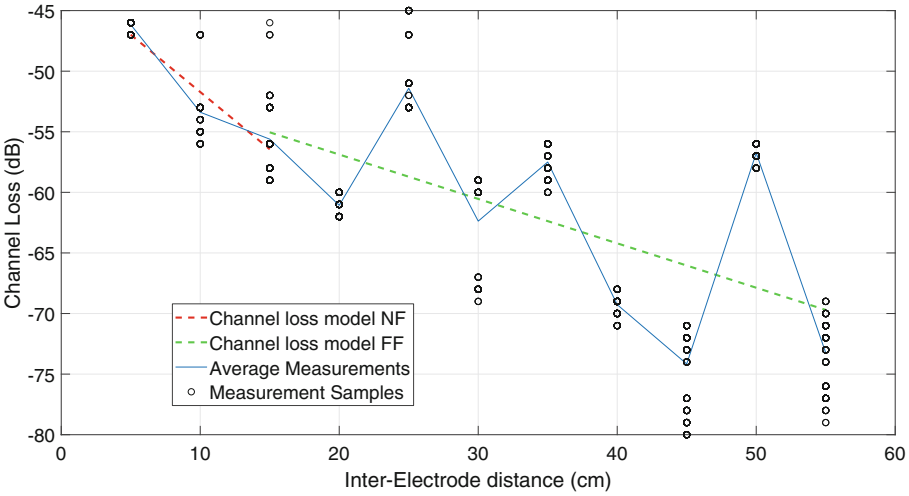

Fig. 14. Channel loss measurements along the arm of a human subject at 450 MHz (black markers). The red and green lines show the two-slope channel loss model described in Eq. 3, fitted to the measurement data. (Color figure online)

Table 1 lists the parameters values of the fit described in Eq. 3 for the following frequencies: 420 MHz, 450 MHz, 480 MHz and 510 MHz.

Table 1. Channel loss parameters.

	420 MHz	450 MHz	480 MHz	510 MHz
L_0 (dB)	−43	−47	−49	−52
α_0 (dB/cm)	−1.2	−0.95	−2.1	−0.79
L_1 (dB)	−54	−55	−62	−59
α_1 (dB/cm)	−0.41	−0.37	−0.19	−0.45
σ (dB)	6.8	6.5	5.8	5.9

Baseline channel loss increased with frequency which is in line with [20]. Near-field losses over distance between 0.8 and 2 dB/cm were measured. These were higher than the far-field losses which were between 0.2 and 0.5 dB/cm. These results are in line with the theoretical model detailed in Sect. 2. It is also interesting to note that the human body is not an homogeneous medium which is the main cause of such an important variance in our measurement results (see Table 1). In fact, the spikes in the channel loss plot in Fig. 14 occur at 25 cm, 35 cm and 50 cm which match the elbow join, the middle of the biceps and the shoulder join of the subject respectively.

Figure 15 shows the Received Signal Strength Indicator (RSSI) while performing on-body measurements for multiple distances over the frequency range

of interest. In this case, the RSSI could be seen as a channel loss since the Tx board was set to transmit at 0 dBm.

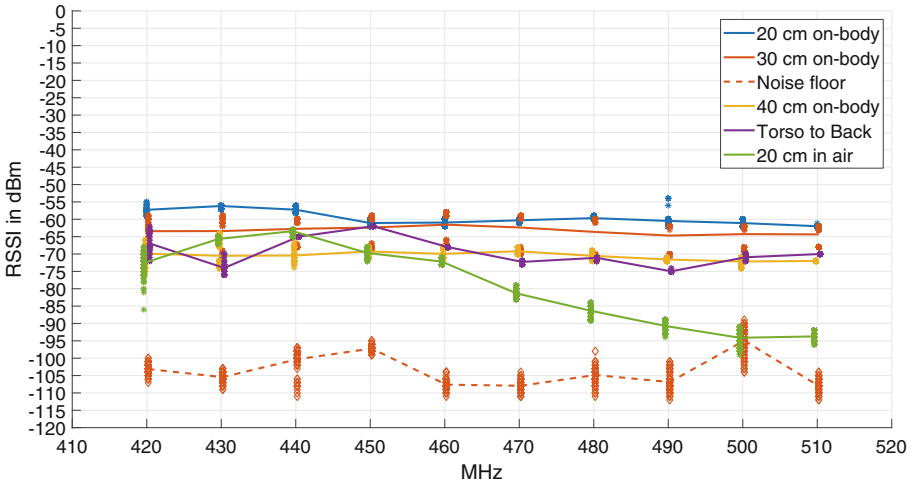

Fig. 15. On-body channel loss for multiple distances.

Figure 15 shows that the variation in on-body channel loss over frequency is relatively small, less than 5 dB over the considered bandwidth over the configurations. This trend over frequency is well aligned with the simulations results from Fig. 11.

Additionally, Fig. 15 shows that the on-body measurements are significantly higher (>30 dB) than the measured noise. This proves that good signal-to-noise can be achieved using C-BCC at these frequencies. To validate the feasibility of C-BCC in conditions where body shielding might occur – such conditions generally lead to the highest on-body channel losses [20] - channel loss was also measured in a back to the torso configuration. The RSSI was found to be higher than the noise and the channel loss did not exceed the one found at 40 cm separation distance. While this result is promising, further research in more non-line of sight conditions has to show whether C-BCC is indeed a good candidate for such communication scenarios. Finally, Fig. 15 also shows the RSSI measured at a separation distance of 20 cm in the air. These were lower than what was measured at 20 cm on the body. This is in line with our numerical simulations and implies that either the electrodes are less efficient in the air or the electrodes are exciting a more efficient communication channel on the body than in the air.

Most previous studies of on-body channel loss at similar frequencies as the ones studied in this manuscript use a channel loss model that is an adaptation of the Friis path loss model with an amended path loss exponent. However, some studies presented on-body propagation measurements at similar frequencies and separation distances as considered in this work, which can be used to extract

average losses per distance. [18] presents numerical values of path loss along the body at 400 MHz that amount to average losses of 0.29 dB/cm between 20 and 55 cm separation distance, reducing to 0.11 dB/cm for larger separation distances between 55 and 100 cm. [9] use a theoretical model that predicts losses for propagation around a cylinder. They found losses per unit distance of 1.1 dB/cm between 20 and 35 cm separation distance at 400 MHz. Finally, using the data that form the basis for the IEEE WBAN standard, presented in [12], a loss per distance of 0.39 dB/cm can be obtained when using the measurements between 40 and 60 cm at 400 MHz. In this work we found far-field losses in between 0.19 dB/cm and 0.45 dB/cm. These values are lower than what is found in [9] since we mainly consider propagation in a relatively straight line. The values found in [18] and [12] fall right in between our measurements.

There are previous studies that have investigated C-BCC. Table 2 shows the comparison of those with this work:

Table 2. Comparison with the State of the Art.

	This work	[17]	[2]	[5]	[13]
BCC Type	Capacitive	Capacitive	Capacitive	Capacitive	Capacitive
Op. freq.	400–500 MHz	0.1–100 MHz	DC-25 MHz	0.1–100 MHz	1–40 MHz
Prop. theory	Yes	No	No	No	No
FS sim.	Yes	No	No	No	No
Phant. sim.	Yes	No	No	No	Yes
Circ. model	No	Yes	No	Yes	No
On-body meas.	Yes	Yes	Yes	Yes	Yes
Bat.powered	Yes (Full)	No	No	Hybrid	No
Elec. size	2×2 cm	2×2 cm	3×3 cm	6×4 cm	$\geq 4 \times 4$ cm
Attenuation	65 dB–30 cm 450 MHz	20 dB–30 cm 100 MHz	75 dB–70 cm @ 25 MHz	45 dB–40 cm @ 100 MHz	25 dB–30 cm @ 40 MHz

5 Perspective and Conclusion

Body Coupled Communication has been demonstrated in a frequency band of 420–510 MHz using three complementary methodologies: theory of radio-frequency (RF) propagation along conductive surfaces such as the human body, simulations of RF propagation along a cuboid muscle phantom, and measurements using a battery-powered prototype on the human body.

The theoretical analysis showed that surface wave excitation is dominant in the envisioned frequency band, leading to a mathematical formulation for the electric fields along the human body. In the far-field of the electrodes, a good agreement is found between this theory and our numerical simulation results.

Ultimately, since the propagation mechanism is dominated by surface waves phenomena at 450 MHz (the frequency of interest), a system implementation

with the same frequency of operation would enable a communication less sensitive to changes of environment since the return path would have almost no impact at this frequency of operation.

Our numerical simulations demonstrated that propagation along a human body phantom depends on the phantoms cross-section and the frequency of operation. The former being a stronger factor.

Finally, we executed on-body channel loss measurements using electrodes and wireless nodes created using off-the-shelf components. These showed higher channel losses in the near field (0.79–2.1 dB/cm) than in the far-field (0.19–0.45 dB/cm), which is in line with theory and our numerical simulations.

Moreover, our measurements demonstrated that in the studied scenario, the received powers are significantly higher than the noise, indicating that wireless communication using this mechanism is suitable to build the human intranet. In addition, C-BCC does not suffer the Body shadowing effect as it is the case for most RF communication solutions.

From a bandwidth perspective, at the frequency of interest (i.e: 450 MHz) the simulations as well as the measurements results highlighted a minimum bandwidth available of 100 MHz over which the attenuation is very close to be constant. This interesting result could benefit our targeted data rate of tens of Mbps and is compatible with ultra-low power wide band solutions.

Future research will focus on electrode development and optimization in order to reduce the base-line channel loss, development of an ASIC and optimization of an on-body network of C-BCC nodes.

References

1. Anderson, G.S., Sodini, C.G.: Body coupled communication: the channel and implantable sensors. In: 2013 IEEE International Conference on Body Sensor Networks, pp. 1–5. IEEE (2013)
2. Arenas, G.M., Gordillo, A.C.: Design and implementation of a body coupled communication system for streaming music. In: 2016 IEEE ANDESCON, pp. 1–4. IEEE (2016)
3. Bae, J., Cho, H., Song, K., Lee, H., Yoo, H.J.: The signal transmission mechanism on the surface of human body for body channel communication. IEEE Trans. Microw. Theory Tech. **60**(3), 582–593 (2012)
4. Chang, T.C., Weber, M.J., Charthad, J., Baltsavias, S., Arbabian, A.: Scaling of ultrasound-powered receivers for sub-millimeter wireless implants. In: 2017 IEEE Biomedical Circuits and Systems Conference (BioCAS), pp. 1–4. IEEE (2017)
5. Cho, N., Yoo, J., Song, S.J., Lee, J., Jeon, S., Yoo, H.J.: The human body characteristics as a signal transmission medium for intrabody communication. IEEE Trans. Microw. Theory Tech. **55**(5), 1080–1086 (2007)
6. Cotton, S.L., D'Errico, R., Oestges, C.: A review of radio channel models for body centric communications. Radio Sci. **49**(6), 371–388 (2014)
7. Das, D., Maity, S., Chatterjee, B., Sen, S.: Enabling covert body area network using electro-quasistatic human body communication. Sci. Rep. **9**(1), 4160 (2019)
8. Elgala, H., Mesleh, R., Haas, H.: Indoor optical wireless communication: potential and state-of-the-art. IEEE Commun. Mag. **49**(9), 56–62 (2011)

9. Fort, A., Keshmiri, F., Crusats, G.R., Craeye, C., Oestges, C.: A body area propagation model derived from fundamental principles: analytical analysis and comparison with measurements. IEEE Trans. Antennas Propag. **58**(2), 503–514 (2009)
10. Gabriel, S., Lau, R., Gabriel, C.: The dielectric properties of biological tissues: III. pParametric models for the dielectric spectrum of tissues. Phys. Med. Biol. **41**(11), 2271 (1996)
11. IEEE, P802.15 Working Group for Wireless Personal Area Networks (WPANs): Channel Model for Body Area Network (BAN), IEEE P802.15-08-0780-09-0006 (2009)
12. Katayama, N., Takizawa, K., Aoyagi, T., Takada, J.I., Li, H.B., Kohno, R.: Channel model on various frequency bands for wearable body area network. IEICE Trans. Commun. **92**(2), 418–424 (2009)
13. Mao, J., Yang, H., Zhao, B.: An investigation on ground electrodes of capacitive coupling human body communication. IEEE Trans. Biomed. Circuits Syst. **11**(4), 910–919 (2017)
14. Mazloum, N.S.: Body-Coupled Communications: Experimental Characterization, Channel Modelling and Physical Layer Design. Chalmers University of Technology (2008)
15. Norton, K.: The propagation of radio waves over the surface of the earth and in the upper atmosphere. Proc. Inst. Radio Eng. **24**(10), 1367–1387 (1936)
16. Norton, K.A.: The propagation of radio waves over the surface of the earth and in the upper atmosphere. Proc. Inst. Radio Eng. **25**(9), 1203–1236 (1937)
17. Pereira, M.D., Alvarez-Botero, G.A., de Sousa, F.R.: Characterization and modeling of the capacitive HBC channel. IEEE Trans. Instrum. Meas. **64**(10), 2626–2635 (2015)
18. Petrillo, L., Mavridis, T., Sarrazin, J., Dricot, J.M., Benlarbi-Delai, A., De Doncker, P.: Ban working frequency: a trade-off between antenna efficiency and propagation losses. In: The 8th European Conference on Antennas and Propagation (EuCAP 2014), pp. 3368–3369. IEEE (2014)
19. Rabaey, J.M.: The human intranet-where swarms and humans meet. IEEE Pervasive Comput. **14**(1), 78–83 (2015)
20. Thielens, A., et al.: A comparative study of on-body radio-frequency links in the 420 MHZ-2.4 GHZ range. Sensors **18**(12), 4165 (2018)
21. Mouser website: Covidien. Kendall ECG electrodes product data sheet. https://www.mouser.com/datasheet/2/813/H124SG-1022817.pdf. Accessed 29 May 2019
22. ST Microelectronics website: Sub-GHZ (430–470 MHz) transceiver development kit based on S2-LP. https://www.st.com/resource/en/data_brief/steval-fki433v2.pdf. Accessed 14 May 2019